Test setup for compressive loading of confined ice thick sections viewed with in-situ cross-polarization imaging

Owen, C.C.; Hammer, T.C.; Hendrikse, H.

Publication date
2022

Document Version
Final published version

Published in
Proceedings of the 26th IAHR International Symposium on Ice

IAHR AIRH

26th IAHR International Symposium on Ice
Montréal, Canada – 19-23 June 2022

Test setup for compressive loading of confined ice thick sections viewed with in-situ cross-polarization imaging

Cody C. Owen[1], Tim C. Hammer[1], Hayo Hendrikse[1]
[1]Delft University of Technology
Faculty of Civil Engineering and Geosciences, Stevinweg 1, 2628CN Delft, The Netherlands
c.c.owen@tudelft.nl, t.c.hammer@tudelft.nl, h.hendrikse@tudelft.nl

For the topic of predicting ice-induced vibrations of vertically sided offshore structures, the rate-dependent ductile-to-brittle transitional deformation and failure behavior of ice is critical but remains superficially understood. To investigate this knowledge gap, a test setup has been designed which allows for in-situ crossed-polarization imaging of passively confined ice thick sections subjected to compressive loading. The test setup is designed to recreate the scenario of a cross-section at the leading edge of an ice sheet which is laterally confined by surrounding ice and fails in crushing against a structure. The setup comprises a linear actuator which drives a flat plate into a confinement box containing the ice thick section, which is passively confined orthogonal to the plane of loading by thick fused silica glass plates. The ice is illuminated through the glass plates with crossed-polarized light, which highlights the microstructure of the ice. Freshwater ice of columnar grain structure is prepared in the ice laboratory at Delft University of Technology, and quantified in terms of its microstructure. The ice thick sections in the test setup are subjected to a range of deformation rates at different temperatures. While similar experiments have been performed, this setup provides novelty by accentuating the dynamic microstructural deformation in-situ with crossed-polarized light. Moreover, this microstructural deformation is observed for global deformation rates relevant for ice-induced vibrations of offshore structures. A description of the test setup is presented along with preliminary experimental results.

1. Introduction

For the topic of predicting ice-induced vibrations of vertically sided offshore structures, the rate-dependent ductile-to-brittle transitional deformation and failure behavior of ice is critical but remains superficially understood. Predictive models of ice-induced vibrations treat the ice-structure interaction phenomenologically, circumventing the detailed complexity of the rate-dependent ice failure and extrusion processes (Hendrikse and Nord 2019; Kärnä, Kamesaki, and Tsukuda 1999). Although the theory of competition between wing-cracks and crack tip plasticity (Schulson and Duval 2009) may be used to explain the ductile-to-brittle transition as part of the global ice failure mechanism in ice-induced vibrations, other theories posit that this transition is not required for ice-induced vibrations to develop (Gagnon 2012). Therefore, it is of interest to investigate whether and how the ductile-to-brittle transition is relevant to the development of ice-induced vibrations, especially for predicting interaction regimes and structural responses of offshore structures such as offshore wind turbines. To this end, the optical property known as birefringence in ice is utilized with crossed-polarized transmitted light to identify the grain structure, also known as microstructure, of thick ice sections under plane-strain compressive loading conditions. Plane-strain conditions of confinement are selected to better simulate the confined compression of ice at the ice-structure interface during dynamic interaction (Frederking 1977; Jordaan et al. 2016). Laboratory-grown S2-type freshwater ice sections are strained at rates in the ductile-to-brittle transition to about 25% while being filmed in crossed-polarized light. The ice laboratory is described, the ice-growing procedure is documented, and the test setup is detailed. Finally, preliminary results are shown with insights on the failure processes during monotonic compressive loading.

2. Delft University Ice Laboratory

The ice laboratory has been in development since April 2020 and is located in Stevin II laboratory at the Faculty of Civil Engineering and Geosciences at Delft University of Technology. The lab consists of two insulated, refrigerated freezer rooms, each with a separate refrigeration system. The colder of the two rooms can achieve temperatures of about -30°C while the warmer can reach about -10°C. The control systems are such that dehumidification cycles result in temperature fluctuations on the order of ±1°C. The rooms are each roughly 2.5 m by 4.5 m with a ceiling height of 2.8 m, excluding the ceiling-mounted evaporator in the center of each room which reduces the height to 2.2 m. The rooms are equipped with a band saw for cutting large ice blocks into manageable sections, heating table for melting ice, ice crusher for making artificial snow, CNC milling machine for programmably producing ice thin sections, polariscope for viewing the ice microstructure, and retrofitted coolers for growing ice blocks. Additionally, the test setup for compressive loading of thick ice sections in crossed-polarized lighting is also installed in the ice laboratory.

3. Laboratory-grown freshwater ice

The ice used in the experiments is grown in the laboratory using Delft tap water. The procedure for growing the ice is as follows. First, tap water at room temperature (around 20°C) is poured into a cooler in the colder room which has been retrofitted with a heated pressure relief system and ball valve at the base for emptying the water when desired. The temperature is set at -20°C and the water surface is left to freeze. Once a thin skim of ice has formed, the ice is removed and an internally-dimensioned 200 mm cubic wooden frame is floated in the water to act as the mold for the shape and size of the ice block desired. Inside the frame is placed either 1) crushed ice or snow sprinkled onto the surface as dry seeding; or 2) a thin ice plate cut from another ice block to act as a template seed from which the ice grain structure will follow during growth (Barrette, Michel, and Stander 1993). The ice is left to grow for between 24 and 72 hours; it was found that roughly 80 mm of ice forms in 24 hours with this setup. After, for example, 72

hours, roughly 180 mm of ice will have grown following the wooden frame, leaving an ideally-shaped cubic ice block free from air bubbles or other optical impurities. The remaining water in the cooler is drained via the ball valve and the wooden frame with ice block is drilled and cut from the surrounding ice in the cooler.

Once removed from the cooler, the wooden frame and ice block are left at room temperature to thaw until the ice block separates from the wooden frame. The ice block is cooled and then cut into plates of about 15 mm thickness with the band saw. These plates can either be vertical or horizontal sections, depending on the type of experiment to be performed. Note that growing the ice to 200 mm thickness takes up to four days and requires as many as five hours to remove from the cooler. Each ice plate is welded to an acrylic plate of similar size with warm tap water. While using warm water melts the bottom surface of the plate slightly, the ice that forms generally follows the grain structure of the ice plate and reduces the likelihood of grain growth emanating from the acrylic plate instead. Once welded to the acrylic, the specimen is milled flat with the CNC milling machine. The acrylic plate is then heated so that the ice can be removed and the machined side is welded to the acrylic. Prior to welding, the machined side is heated with a hair dryer to melt the milling grooves and lines and promote a smoother surface for welding. Once the machined side is welded to the acrylic, the specimen is machined a target thickness of 10.50 mm or 5.20 mm with a machining tolerance of ±0.20 mm over 200 mm and an accuracy of 0.05 mm. The ice thick section is then removed from the acrylic and the machined surface is heated with the aforesaid method, and then the uneven edges from the welding are melted flat. The dimensions of the thick section are measured and a series of photographs are taken of the thick section rotated through the azimuth in the polariscope. An example of an ice thick section is shown in Figure 1.

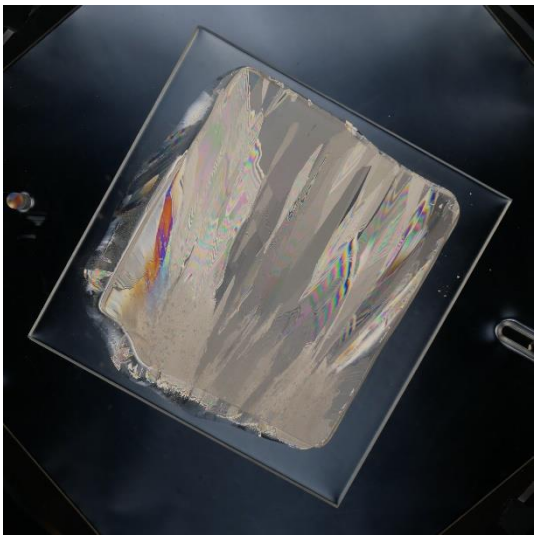

Figure 1. Example photograph of a vertical thick section of S2-type freshwater ice with crossed-polarized transmitted light. The acrylic plate to which the ice is welded is 220 mm square.

4. Test setup

The test setup was inspired by the experiments performed for relatively high-speed crushing of confined ice (Gagnon and Bugden 2007, 2008) as well as from some previous, related experiments (Fransson, Olofsson, and Sandkvist 1991; Gagnon 1994). While the focus of previous experiments was mainly on the local pressures at the ice-structure interface, an indubitably important venture, a key aspect of the interaction was not deeply appreciated: the

ice deformation and failure beyond the interface. Besides viewing the formation and propagation of cracks, optically pure ice in unpolarized transmitted light shows nothing more about the stress state or accommodation. It was decided to view the ice in crossed-polarized transmitted light as is typically done in polariscopes or polarization microscopes with thin sections for ice texture analysis (e.g. Gagnon (1998)). By using crossed-polarized light, not only is the microstructure made visible in the ice, but also elastic-stress-induced birefringence changes in the microstructure can be identified and measured (Ravi-Chandar et al. 1994).

Following these ideas, a test setup was designed and built which subjects an ice thick section to passive plane-strain compressive loading while being observable in crossed-polarized transmitted light (see Figure 2). The test setup is called the Optical apparatus with Linear Actuator loading Frame (OLAF) and consists of two main components: 1) the confinement box, and 2) the loading frame. The confinement box comprises a T-shaped backing steel plate to which the aluminium frames are mounted. The aluminium frames house the 40-mm-thick fused-silica glass plates, between which the ice plate is inserted. The glass plates float on rubber seals and are held in place loosely by the seals and tightly by the ice plate. The confinement box is held together by seven steel bolts which are removed to dismantle the box, which weighs about 35 kg in total. The T-shaped backing steel plate sets the gap between the glass plates and therefore matches the ice plate thickness; this gap can be either 5.0 mm or 10.0 mm depending on the configuration chosen (from the 5-mm-backing plate or the 10-mm-backing plate). Opposite the backing plate is the opening of the box which has printed-plastic guides. The loading frame comprises an extruded aluminium base, upon which a solid aluminium base plate is mounted. Opposite to the base plate is the linear electric actuator (GSX50-1005-MKR-SB5-358-G2ACTUATION DIVISION-EXLAR Corporation, Eden Prairie MN 55346, USA) with indentor plate. The indentor plate is connected to the actuator via a bearing and guide system which transfers only in-line translational motion and force to the indentor plate. The torque generated by the actuator is absorbed by the frame via the actuator torque compensator. Force is measured with a load cell (VST5000 S-type load cell, HENK MAAS Weegschalen B.V., 4264 AW Veen, The Netherlands) between the actuator and the indentor plate. The displacement of the actuator or indentor plate is measured by a magneto-strictive displacement sensor (BIW0007-BIW1-A310-M0250-P1-S115 Balluff B.V., 5232 BC ‘s-Hertogenbosch, The Netherlands). The actuator, load cell, displacement sensor, and control system were adapted from the test setup used in the SHIVER project (Hammer et al. 2021).

The confinement box is installed via weight-compensated crane onto the base plate with a bolted connection and alignment pins, and the indentor plate enters the confinement box between the printed-plastic guides. All loads are self-contained internally by the loading frame, and the whole setup is placed on a wooden pallet for mobility. Given that the floor of the ice laboratory is insulated and limited to 1000 kg m^{-2}, the design was made to be as light, rigid, and self-contained as possible such that no floor anchoring was necessary. The whole setup weighs about 350 kg and can be moved by manual pallet cart with ease. During the experiments, linearly-polarized light is transmitted through the glass plates by an LED light panel (JINBEI EFP-50 BICOLOR LED PANEL LIGHT, RCP Handels-GmbH & Co. KG, in de Tarpen 42, D-22848 Norderstedt, Germany) on an adjustable stand and covered with a linear polarizer sheet (300 x 300 mm linear polarizing film XP42-40, Edmund Optics Ltd., Unit 1, Opus Avenue, Nether Poppleton York, YO26 6BL, United Kingdom). The ice plate is deformed by the indentor plate at, e.g., a constant displacement rate, the displacement of the indentor and the force on the indentor are measured by the displacement sensor and the load cell, respectively. The deformation process of the ice is captured by two video cameras at 2.7K resolution and 50 frames per second (GoPro HERO9 Black, 3025 Clearview Way, San Mateo,

CA 94402, USA) with linear polarizers over the lenses oriented 90° to the polarizer on the LED light panel.

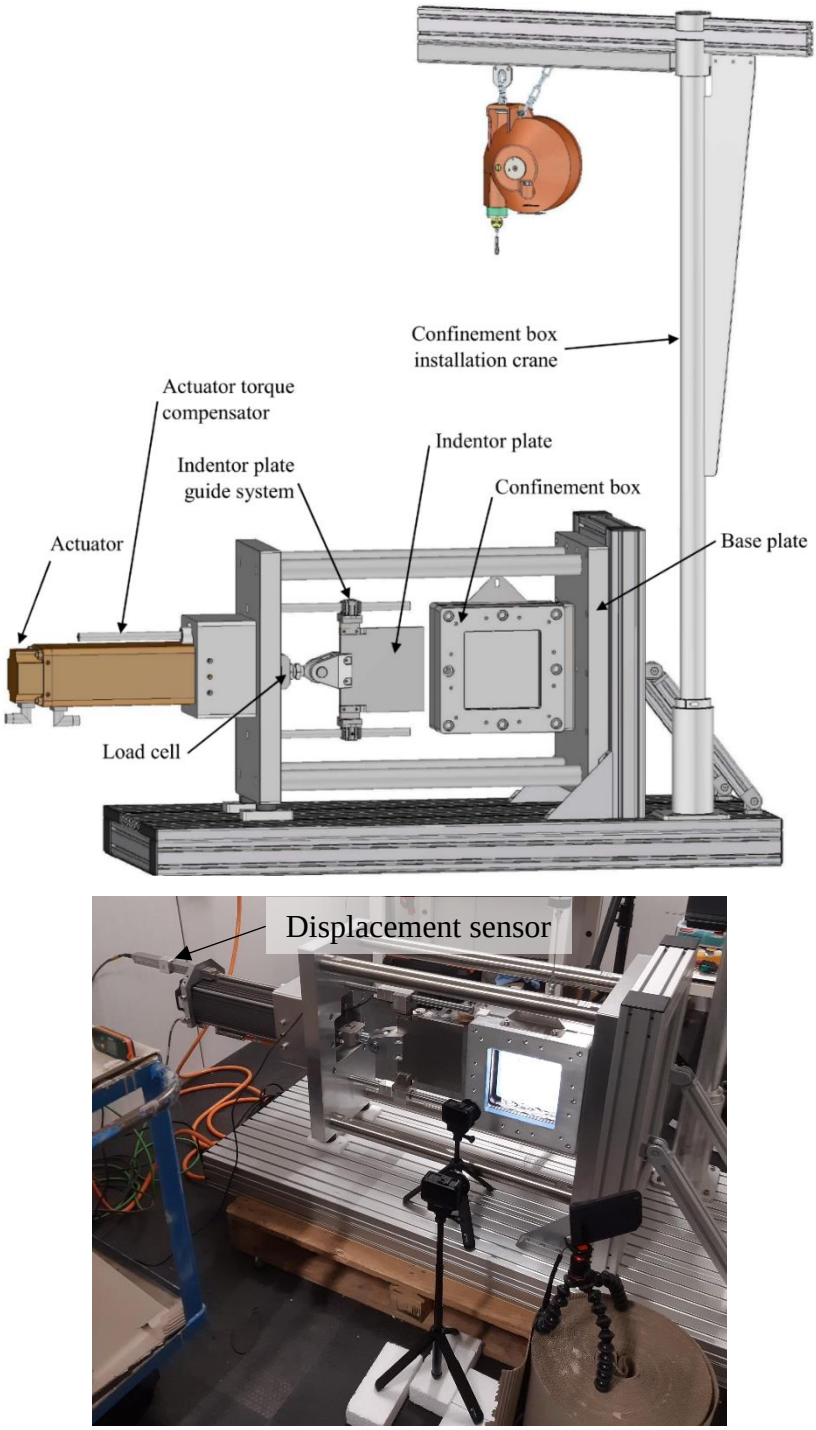

Figure 2. Test setup. Top: schematic of test setup. Bottom: photograph of test setup in the ice laboratory. Note that the displacement sensor is connected to the actuator torque compensator and light is shone through the glass plates of the confinement box and the view of the window is recorded with two video cameras.

5. Preliminary results

The following preliminary results from the experimental campaign for this test setup pertain to a test with a vertical section of S2-type freshwater ice compressed at a nominal rate of

0.02 mm s^{-1} ($\dot{\varepsilon}_{nom} = 1 \cdot 10^{-4}\ s^{-1}$). Nominal strain rate $\dot{\varepsilon}_{nom}$ is calculated as the displacement of the indentor plate normalized by the length of the undeformed ice plate (200 mm). This strain rate is selected due to the apparent ductile-to-brittle transitional behavior observed in indentation as well as uniaxial and biaxial compression of freshwater S2-type ice (Grape and Schulson 1992; Iliescu and Schulson 2004; Schulson and Buck 1995). The test was performed at an air temperature of -7±1°C, which is deemed representative of the ice temperature since the ice was equilibrated at this air temperature for at least six hours. All data were collected at 100 Hz sampling rate and are shown unfiltered. The time histories of indentor displacement and force (compression shown as positive values) for this test are shown in Figure 3, and the corresponding stress-strain curve is shown in Figure 4. The nominal stress is calculated as the force divided by the nominal contact area between the indentor plate and the ice plate (ice thickness by height of ice plate). For this test, the ice thickness is approximately 5 mm and the height of the ice plate is approximately 170 mm.

Within the first 200 seconds, the ice plate is loaded and deforms elastically, then fails in a brittle manner at a nominal pressure of 4.0 MPa with a subsequent load drop. Following this brittle-elastic behavior, the ice plate is reloaded and proceeds to deform seemingly plastically, with global deformation acting in a flowing manner but with local microcracking and pulverization. After about 1800 seconds in Figure 3, it can be seen that the displacement halts for a period then continues increasing. This was caused by a time-out error in the controller which required user input to resume; while erroneous, it is interesting to observe the stress relaxation. Ultimately, the highest force was reached, and highest stress of 6.4 MPa, at the end of the test at highest nominal strain when the ice plate was deformed 24.4%. The ice was significantly damaged (microstructural changes like microcracks, cracks on the order of the size of the grain diameter, and material separation or rotation) such that microstructurally the material behaved differently from the original state of the ice (see Figure 5). Much of the damage at the end of the test had been contained locally in the shear fault (A) that developed during the brittle-elastic failure at around 0.7% nominal strain. Besides the damage in the shear fault, non-interacting microcracks in the direction of compression formed randomly spatiotemporally throughout the ice plate. The general increase in the force after the brittle-elastic failure is mainly caused by the change in geometry of the ice plate and some added confinement from the alignment rings located between the aluminium plates holding the glass plates. These alignment rings are positioned where the bolts are inserted on the upper and lower middle part of the confinement box. This added confinement begins to play a role in the stress-strain history after around 1400 seconds when there is a clear increasing trend in the force.

A series of frames of the video from the test is shown in Figure 5, which correspond to the time instances labeled in Figure 4. The interference colors at the corners of the window are from the stress-induced birefringence of the glass plates and not from the ice itself; the interference colors for ice of 5 mm thickness are mainly varying shades of grey. Additionally, some cracks can be observed around the periphery of the ice plate in frame 1, this was caused by the installation of the ice plate in the confinement box when the bolts were tightened. The ice plate is milled to a thickness greater than the gap between the glass plates, and when the bolts are tightened to secure the box, the glass plates confine the ice and can cause the ice to crack. Ideally, the tolerance on the machining would be such that the ice does not crack, but this is difficult to attain with the current equipment.

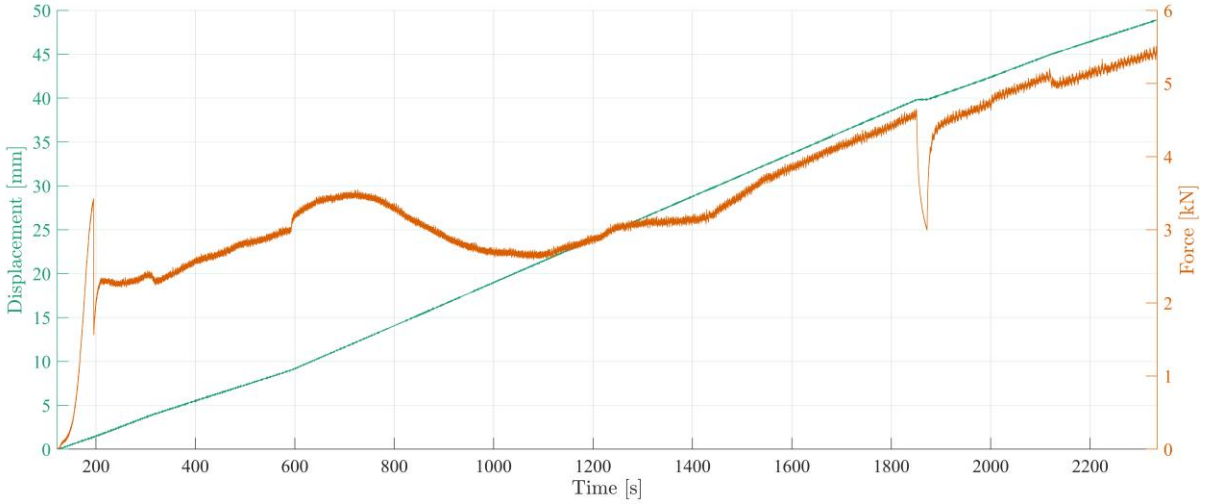

Figure 3. Example time histories of indentor displacement (left) and force (right) for a plane-strain compression of a vertical thick section of S2-type freshwater ice at a nominal strain rate of $\dot{\varepsilon}_{nom} = 1 \cdot 10^{-4}\ s^{-1}$ and at an air temperature of -7±1°C.

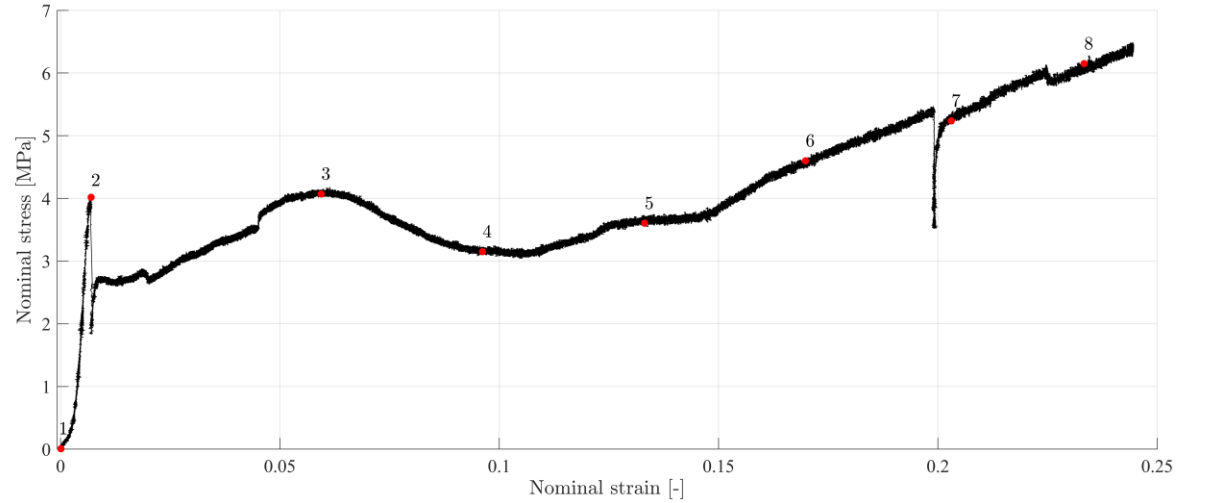

Figure 4. The nominal stress-strain curve corresponding to the time histories of force and displacement from Figure 3. The red markers with number labels correspond to the video frames in Figure 5.

As previously mentioned, the damage that developed after brittle failure mainly occurred around the shear fault beginning in frame 2, with microcracking distributed uniformly throughout the ice plate. Some ice grains were minimally altered overall, containing some microcracking but remain mostly transparent as in frame 1. Moreover, the interference color of those mostly unaltered grains does not appear to change after frame 2, when brittle failure occurred. This suggests that the microstructural modifications are heterogeneous and strain localizes in damaged regions such as the shear fault, as observed elsewhere (Chauve et al. 2017).

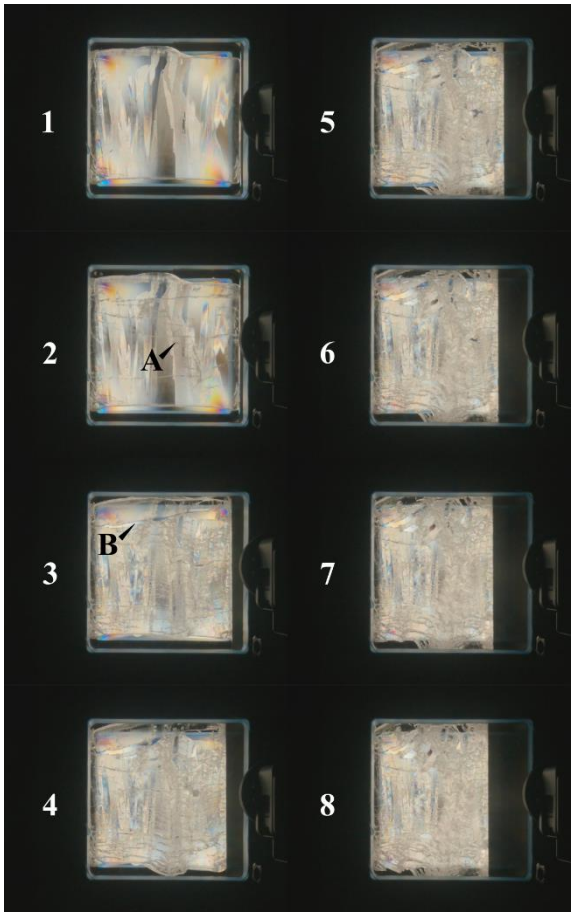

Figure 5. Video frames from the test at time instances corresponding to the labeled markers in Figure 4. The shear fault is labeled A in frame 2. An example of cleavage fracture resulting in a gap in the ice plate is labeled B in frame 3.

6. Discussion

The test setup provides a method for simultaneously measuring and observing deformation and failure behavior of passive plane-strain compressive loading of ice. While preliminary, the results demonstrate that the global mechanical behavior of the ice differs substantially between the brittle linear-elastic manner within the initial 1% strain and the plastic, ductile-like manner thereafter. Interestingly, local behavior throughout the ice plate after 1% strain appears brittle with microcracking and separation or rotation of crushed material, but the global behavior appears ductile, or at least not brittle, in terms of the load history. Perhaps the ductile-to-brittle transitional behavior can be better defined in terms of scales of behavior: locally, brittle behavior is observed; and globally, non-brittle behavior is observed. The transition is then a change in contribution of ductile and brittle mechanics based on scale, where at lower strain rates both scales are ductile, at higher strain rates both scales are brittle, and for intermediate strain rates, local-scale brittleness is observed while global-scale ductility is observed. Note that these trends are also dependent on temperature and grain size, among other factors.

The confinement of the ice is not explicitly known, since the plane-strain scenario is maintained by the rigidity of the glass plates and the stress on the ice from the glass plates is not measured. Additionally, once the ice fractured at 0.7% nominal strain, any assumption of Poisson ratio defining the stress from the glass plates is no longer valid. This is especially the case where cleavage fractures occurred and gaps (B) between the ice are seen, such as in frame 3 in Figure 5. For the test setup, it has been suggested to add side-lighting to visibly enhance the ice fracture

surfaces during deformation, a technique which has been applied to viewing thin sections of microstructurally damaged ice (Melanson et al. 1999).

For dynamic ice-structure interaction, the ice that interacts with the structure is significantly damaged, suggesting that uni-, bi-, or tri-axial compression tests with undamaged ice may not be representative of the material which interacts with the structure. Instead, it is the damaged, or microstructurally modified, ice which can govern the interaction. Ice constitutive models and ice-induced vibration models have considered this observation of damage, which further substantiates this claim (Morsy 1995; Singh and Jordaan 1999; Weiss and Dansereau 2017; Xiao and Jordaan 1996). It is therefore recommended that both intact and damaged ice properties are considered in constitutive and otherwise phenomenological modeling of ice for dynamic ice-structure interaction modeling. It is likely the case that the damaged ice is better representative of long-term, continuous ice-structure interaction rather than intact ice.

7. Conclusion

For the topic of predicting ice-induced vibrations of vertically sided offshore structures, the rate-dependent ductile-to-brittle transitional deformation and failure behavior of ice is critical but remains superficially understood. To investigate this knowledge gap, a test setup has been designed which allows for in-situ crossed-polarization imaging of passively confined ice thick sections subjected to compressive loading. The test setup provides a novel method for simultaneously measuring and observing deformation and failure behavior of passive plane-strain compressive loading of ice, which can offer insight into dynamic ice-structure interaction with focus on the ice. Based on preliminary results, it is recommended that both intact and damaged ice properties are considered in the implementation of constitutive and phenomenological modeling of ice in dynamic ice-structure interaction.

Acknowledgments

The authors thank the participating organizations in the SHIVER project: TU Delft, Siemens Gamesa Renewable Energy, and Aalto University, for supporting this work. The SHIVER project is co-financed by Siemens Gamesa Renewable Energy and TKI-Energy by the ‘Toeslag voor Topconsortia voor Kennis en Innovatie (TKI’s)’ of the Dutch Ministry of Economic Affairs and Climate Policy. The authors also thank Jeroen Koning for the detailed design and logistics for the fabrication of the test setup, and Kees van Beek for assisting in adapting the ELSA control system to this application.

References

Barrette, Paul, Bernard Michel, and Edward Stander. 1993. “On the Reproduction of Ice from a Common Seed.” *Journal of Crystal Growth* 131(1–2):153–56.

Chauve, Thomas, Maurine Montagnat, Cedric Lachaud, David Georges, and Pierre Vacher. 2017. “Strain Field Evolution at the Ductile-to-Brittle Transition: A Case Study on Ice.” *Solid Earth* 8(5):943–53.

Fransson, Lennart, Thomas Olofsson, and Jim Sandkvist. 1991. “Observations of the Failure Process in Ice Blocks Crushed by a Flat Indentor.” Pp. 501–14 in *Proceedings of the 11th International Conference on Port and Ocean Engineering under Arctic Conditions*. Vol. 1, edited by D. B. Muggeridge, D. B. Colbourne, and H. M. Muggeridge. St. John’s, Canada: POAC.

Frederking, R. 1977. “Plane-Strain Compressive Strength of Columnar-Grained and Granular-Snow Ice.” *Journal of Glaciology* 18(80):505–16.

Gagnon, R. E. 1994. “Generation of Melt during Crushing Experiments on Freshwater Ice.” *Cold Regions Science and Technology* 22(4):385–98.

Gagnon, R. E. 1998. “Analysis of Visual Data from Medium Scale Indentation Experiments at Hobson’s Choice Ice Island.” *Cold Regions Science and Technology* 28(1):45–58.
Gagnon, R. E. 2012. “An Explanation for the Molikpaq May 12, 1986 Event.” *Cold Regions Science and Technology* 82:75–93.
Gagnon, R. E. and A. Bugden. 2007. “Ice Crushing Tests Using a Modified Novel Apparatus.” Pp. 235–44 in *Proceedings of the 19th International Conference on Port and Ocean Engineering under Arctic Conditions*. Vol. 1. Dalian, China: POAC.
Gagnon, R. E. and A. Bugden. 2008. “2-Dimensional Edge Crushing Tests on Thick Sections of Ice Confined at the Section Face.” Pp. 973–91 in *Proceedings of the 19th IAHR International Symposium on Ice*. Vol. 2. Vancouver, British Columbia, Canada: IAHR.
Grape, Johan A. and Erland M. Schulson. 1992. “Effect of Confining Stress on Brittle Indentation Failure of Columnar Ice.” *International Journal of Offshore and Polar Engineering* 2(3):212–21.
Hammer, Tim C., Kees van Beek, Jeroen Koning, and Hayo Hendrikse. 2021. “A 2D Test Setup for Scaled Real-Time Hybrid Tests of Dynamic Ice- Structure Interaction.” Pp. 1–13 in *Proceedings of the 26th International Conference on Port and Ocean Engineering under Arctic Conditions*. Moscow, Russia: POAC.
Hendrikse, Hayo and Torodd S. Nord. 2019. “Dynamic Response of an Offshore Structure Interacting with an Ice Floe Failing in Crushing.” *Marine Structures* 65:271–90.
Iliescu, Daniel and Erland M. Schulson. 2004. “The Brittle Compressive Failure of Fresh-Water Columnar Ice Loaded Biaxially.” *Acta Materialia* 52(20):5723–35.
Jordaan, Ian, Brian O’Rourke, Joshua Turner, Perry Moore, and Freeman Ralph. 2016. “Estimation of Ice Loads Using Mechanics of Ice Failure in Compression.” Pp. 1–12 in *Arctic Technology Conference 2016*. St. John’s, Newfoundland and Labrador, Canada: OTC (ATC).
Kärnä, T., K. Kamesaki, and H. Tsukuda. 1999. “Numerical Model for Dynamic Ice-Structure Interaction.” *Computers and Structures* 72(4):645–58.
Melanson, P. M., I. L. Meglis, I. J. Jordaan, and B. M. Stone. 1999. “Microstructural Change in Ice: I. Constant-Deformation-Rate Tests under Triaxial Stress Conditions.” *Journal of Glaciology* 45(151):417–22.
Morsy, Usama Abd-Elmoaty. 1995. “Non-Linear Finite Element Modelling of Dynamic Loads on Offshore Structures.” University of Calgary.
Ravi-Chandar, K., B. Adamson, J. Lazo, and J. P. Dempsey. 1994. “Stress-Optic Effect in Ice.” *Applied Physics Letters* 64(10):1183–85.
Schulson, E. M. and S. E. Buck. 1995. “The Ductile-to-Brittle Transition and Ductile Failure Envelopes of Orthotropic Ice under Biaxial Compression.” *Acta Metallurgica et Materialia* 43(10):3661–68.
Schulson, Erland M. and Paul Duval. 2009. *Creep and Fracture of Ice*. Cambridge University Press.
Singh, S. K. and I. J. Jordaan. 1999. “Constitutive Behaviour of Crushed Ice.” *International Journal of Fracture* 97(1–4):171–87.
Weiss, Jérôme and Véronique Dansereau. 2017. “Linking Scales in Sea Ice Mechanics.” *Philosophical Transactions of the Royal Society A: Mathematical, Physical and Engineering Sciences* 375(20150352):17.
Xiao, J. and I. J. Jordaan. 1996. “Application of Damage Mechanics to Ice Failure in Compression.” *Cold Regions Science and Technology* 24(3):305–22.